An additive algorithm for origami design

Levi H. Dudte[a], **Gary P. T. Choi**[a,b], **and L. Mahadevan**[a,c,d,1]

[a]John A. Paulson School of Engineering and Applied Sciences, Harvard University, Cambridge, MA 02138; [b]Department of Mathematics, Massachusetts Institute of Technology, Cambridge, MA 02139; [c]Department of Physics, Harvard University, Cambridge, MA 02138; and [d]Department of Organismic and Evolutionary Biology, Harvard University, Cambridge, MA 02138

Edited by Andrea J. Liu, University of Pennsylvania, Philadelphia, PA, and approved March 5, 2021 (received for review September 11, 2020)

Inspired by the allure of additive fabrication, we pose the problem of origami design from a different perspective: How can we grow a folded surface in three dimensions from a seed so that it is guaranteed to be isometric to the plane? We solve this problem in two steps: by first identifying the geometric conditions for the compatible completion of two separate folds into a single developable fourfold vertex, and then showing how this foundation allows us to grow a geometrically compatible front at the boundary of a given folded seed. This yields a complete marching, or additive, algorithm for the inverse design of the complete space of developable quad origami patterns that can be folded from flat sheets. We illustrate the flexibility of our approach by growing ordered, disordered, straight, and curved-folded origami and fitting surfaces of given curvature with folded approximants. Overall, our simple shift in perspective from a global search to a local rule has the potential to transform origami-based metastructure design.

origami | computational design | metamaterials | additive fabrication

Folding patterns arise in nature in systems including insect wings, leaves, and guts (1–4) and have a long history in decorative, ceremonial, and pedagogical traditions of origami around the world. More recently, they have begun to draw the attention of mathematicians fascinated by the patterns and limits of folding (5–9) and engineers and scientists inspired by their technological promise (10–18).

The simplest origami is a single vertex with four folds, a kind of hydrogen atom of folding with exactly one internal degree of freedom (DOF). Patterns comprising four-coordinated vertices and quadrilateral faces are called quad origami, which may have isolated folded configurations isometric to the plane, if they can be folded at all. The mechanical response of structures and materials derived from quad origami is governed in large part by geometric frustration encountered during folding. Using these patterns to program rigid-foldable and flat-foldable, floppy, or multistable systems then requires consideration of additional symmetries (19) and folds (20), making quad origami a promising platform for metastructures at any scale from the nanoscopic to the architectural. This has attracted significant scientific interest to the problem of their design, but the challenge of either finding quad patterns that actually fold or, inversely, surfaces that unfold has limited freeform solutions.

Previous quad origami design studies have tended to focus on tessellations with periodic geometries and specific mountain/valley (MV) assignments assumed a priori, with the well-known Miura-ori pattern (21) being the canonical example, and have generally employed either direct geometric methods to parameterize simple design variations (22–30) or optimization algorithms to generalize known folding typologies (31–34). The former typically provide a comprehensive understanding of a restricted space of designs sharing strong qualitative similarities—i.e., those exhibiting particular symmetries—and involve constructions that are inevitably case-specific. The latter typically require encoding nonlinear developability constraints in a nonconvex, multidimensional optimization framework and use a well-known periodic folding pattern as an empirical departure point. These computational methods are generic, but they suffer from two problems: the difficulty of finding a good guess to ensure convergence to a desired local solution and the lack of scalability to large problems. Thus, while many current strategies have been used to expound on a wide variety of quad origami patterns, the general problem of quad origami design has admitted only piecemeal solutions, and the science has, for the most part, followed the art form.

Inspired by the simple edge-extrusion operation from computational design and additive fabrication, one can ask the following inverse problem: How can we extend the boundary of a folded quad origami surface outward such that the new surface remains developable—i.e., isometric to the plane and thus capable of being fabricated from flat sheets? In the case of origami, this implies that a folding process can transform the pattern through intermediate configurations to a second global energy minimum, the designed, folded surface. Although this typically implies geometric frustration in intermediate stages, recently, several marching algorithms have been developed to design quad origami that, in addition to developing to the plane, can deploy rigidly—i.e., with no geometric frustration. This allows for deployment from a flat to folded to flat-folded configurations with one DOF, a subclass of developable quad origami known as rigid- and flat-foldable (35–37), such as a "jigsaw" method to design rigid-foldable quad origami (36), a combinatorial strategy borrowed from artistic modular origami design (38), wherein geometrically compatible folded units are selected from a predetermined set of discrete modules to augment the boundary of a folded bulk model.

Here, we deviate fundamentally from these previous approaches by providing a unified framework that identifies the complete continuous family of compatible, folded strips

Significance

Origami, the art of paper folding, is an emerging platform for mechanical metamaterials. Prior work on the design of origami-based structures has focused on simple geometric constructions for limited spaces of origami typologies or global constrained optimization problems that are difficult to solve. Here, we reverse the mathematical, computational, and physical paradigm of origami design by proposing a simple local marching approach that leads to a constructive theorem on the geometry of compatible growth directions at the boundary of a given folded seed. We show how this discovery yields a simple algorithm for the additive design of all developable quadrilateral surfaces, enabling the design of novel foldable metastructures from flat sheets at any scale.

Author contributions: L.H.D. and L.M. conceived the research; L.H.D., G.P.T.C., and L.M. designed the research; L.H.D. derived the theoretical results; L.H.D. and G.P.T.C. implemented the algorithms and conducted the numerical experiments; L.H.D., G.P.T.C., and L.M. analyzed the results; and L.H.D., G.P.T.C., and L.M. wrote the manuscript.

Competing interest statement: L.H.D. and L.M. have filed a patent on the proposed algorithm for origami design.

This article is a PNAS Direct Submission.

[1]To whom correspondence may be addressed. Email: lmahadev@g.harvard.edu.

This article contains supporting information online at https://www.pnas.org/lookup/suppl/doi:10.1073/pnas.2019241118/-/DCSupplemental.

Published May 17, 2021.

that can be extruded directly from the boundary of a folded model. This lays the foundation for an algorithm that allows us to explore the entire space of developable quad origami designs, not limited to just rigid- and/or flat-foldable designs. We begin by exploring the flexibility in angles and lengths associated with fusing two pairs of folded faces at a common boundary, which yields the geometric compatibility conditions for designing a four-coordinated, single-vertex origami. We then apply the single-vertex construction to determine the space of compatible quad origami strips at the boundary of an existing folded model. Critically, we establish that the new interior edge directions and design angles along the growth front form a one-dimensional family parameterized by the choice of a single face orientation in space along the growth front. The result is an additive geometric algorithm for the evolution of folded fronts around a prescribed seed into a folded surface, establishing the means to characterize the entire design space of generic quad origami surfaces. This constructive algorithm (39) is enabled by the following:

Theorem. *The space of new interior edge directions along the entire growth front in a quad origami is one-dimensional—i.e., uniquely determined by a single angle*.

Proof: Our proof primarily consists of three parts: single-vertex construction, construction of adjacent vertices, and the growth of the full growth, with details given in *SI Appendix*, section S1.

1. Single-vertex construction: Suppose we are given a vertex along the growth front with position vector $\mathbf{x}_i$ (Fig. 1*A*), with the two adjacent growth-front vertices denoted by $\mathbf{x}_{i-1}, \mathbf{x}_{i+1}$. We denote the two boundary-design angles incident to $\mathbf{x}_i$ in the existing surface by $\theta_{i,3}$ and $\theta_{i,4}$ and the angle in space at $\mathbf{x}_i$ along the growth front denoted by $\beta_i = \angle\{-\mathbf{e}_i, \mathbf{e}_{i+1}\} \in (0, \pi)$ (Fig. 1*B*), where $\mathbf{e}_i = \mathbf{x}_i - \mathbf{x}_{i-1}$ and $\mathbf{e}_{i+1} = \mathbf{x}_{i+1} - \mathbf{x}_i$. To

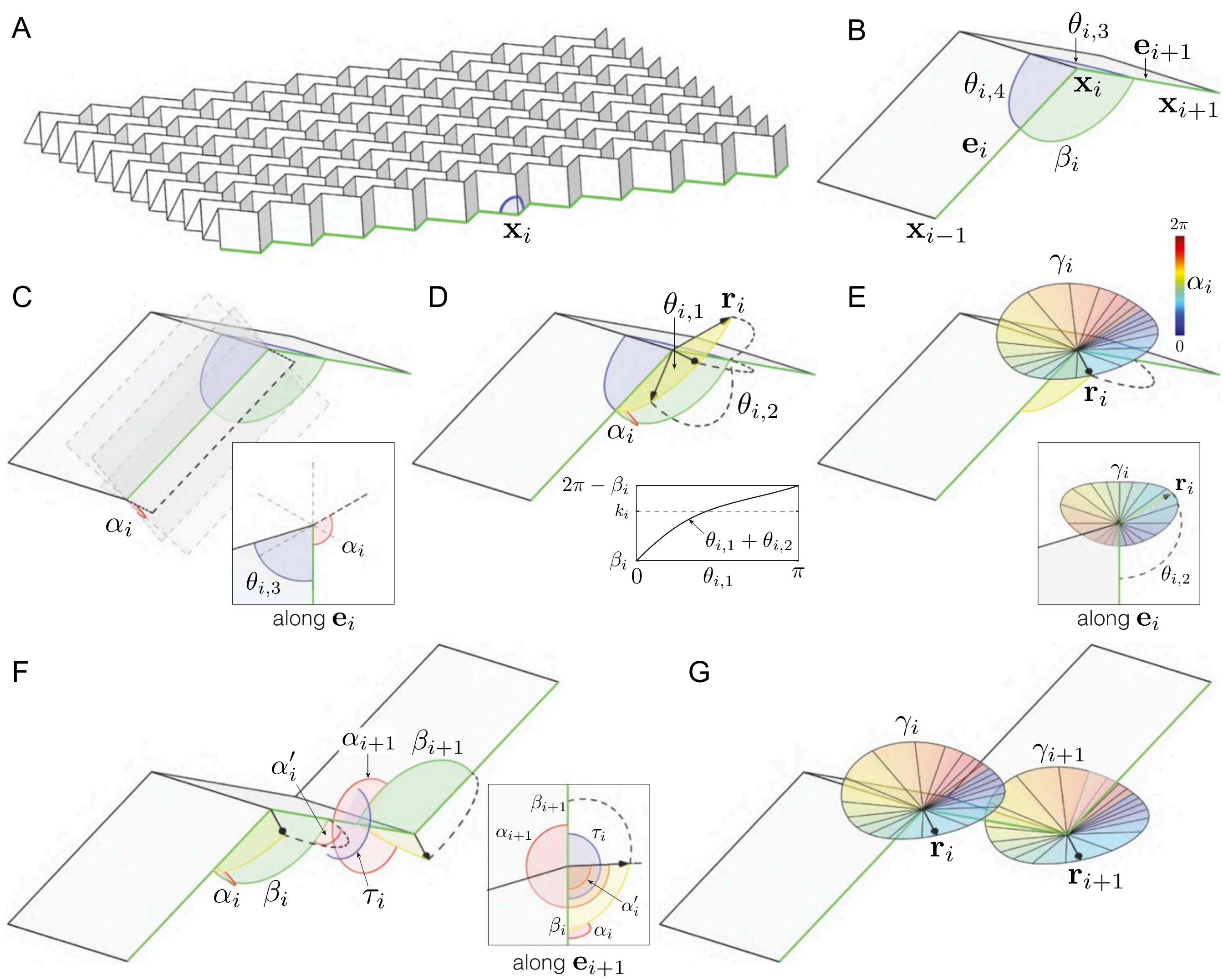

Fig. 1. Construction of quad origami. (*A*) A quad origami surface, the Miura-ori pattern, with boundary vertex $\mathbf{x}_i$ along a growth front (green). (*B*) Focusing on $\mathbf{x}_i$, shown from a different vantage point than that of *A*, its adjacent growth-front vertices $\mathbf{x}_{i-1}$ and $\mathbf{x}_{i+1}$. The two design angles along the boundary $\theta_{i,3}$ and $\theta_{i,4}$ are shown in blue, and the angle in space β_i between the two growth-front edges $\mathbf{e}_i$ and $\mathbf{e}_{i+1}$ is in green. (*C*) The plane of action for new design angle $\theta_{i,1}$ is determined by a flap angle α_i (red), which sweeps from the β_i face clockwise about $\mathbf{e}_i$. (*D*) As $\theta_{i,1}$ (yellow) sweeps through its plane of action, it determines possible growth directions $\mathbf{r}_i$ and $\theta_{i,2}$ (dashed), the angle between $\mathbf{r}_i$ and $\mathbf{e}_{i+1}$. These must satisfy $\theta_{i,1} + \theta_{i,2} = k_i$ (*D*, *Inset*) to create a developable vertex $\mathbf{x}_i$. (*E*) This constraint gives an ellipse γ_i of spherical arcs $\theta_{i,1}$ and $\theta_{i,2}$, which forms a closed loop around the line containing $\mathbf{e}_i$. The value of $\theta_{i,1}$ that satisfies the constraint is given by the unique intersection of its plane of action and γ_i, so α_i parameterizes γ_i. (*F*) The secondary flap angle α_i' at $\mathbf{x}_i$ sweeps from the β_i face clockwise about $\mathbf{e}_{i+1}$ and is determined by α_i. The flap angle α_{i+1} at $\mathbf{x}_{i+1}$ sweeps from the β_{i+1} face clockwise about $\mathbf{e}_{i+1}$ to the same plane as measured by α_i'. (*G*) Two adjacent growth directions $\mathbf{r}_i$ and $\mathbf{r}_{i+1}$ must be coplanar, so $\mathbf{r}_{i+1}$ is determined by the intersection of this plane and γ_{i+1}; thus, α_{i+1} parameterizes γ_{i+1}.

obtain a new edge-direction vector $\mathbf{r}_i$ that gives the direction of an interior edge $[\mathbf{x}_i, \mathbf{x}_i']$ in the augmented quad origami surface, let $\alpha_i \in [0, 2\pi)$ be the left-hand-oriented flap angle about $\mathbf{e}_i$ from the β_i plane to the plane of the new quad containing $\mathbf{r}_i$ and $\mathbf{e}_i$ (Fig. 1*C*). We note that the single-vertex origami at $\mathbf{x}_i$ satisfies the local-angle sum developability condition

$$\sum_{j=1}^{4} \theta_{i,j} = 2\pi, \qquad \textbf{[1]}$$

where $\theta_{i,1} = \angle\{-\mathbf{e}_i, \mathbf{r}_i\} \in (0, \pi)$ and $\theta_{i,2} = \angle\{\mathbf{e}_{i+1}, \mathbf{r}_i\} \in (0, \pi)$ are two new design angles implied by $\mathbf{r}_i$ (Fig. 1*D*). Furthermore, $\theta_{i,1}$, $\theta_{i,2}$, and β_i form a spherical triangle with α_i an interior spherical angle opposite $\theta_{i,2}$, so that the spherical law of cosines gives

$$\cos\theta_{i,2} = \cos\theta_{i,1}\cos\beta_i + \sin\theta_{i,1}\sin\beta_i\cos\alpha_i. \qquad \textbf{[2]}$$

Solving Eqs. **1** and **2** for $\theta_{i,1}, \theta_{i,2}$ yields

$$\theta_{i,1} = \tan^{-1}\frac{\cos k_i - \cos\beta_i}{\sin\beta_i\cos\alpha_i - \sin k_i},\ \theta_{i,1} \neq \pi/2, \qquad \textbf{[3]}$$

$$\theta_{i,2} = k_i - \theta_{i,1}, \qquad \textbf{[4]}$$

where $k_i = 2\pi - \theta_{i,3} - \theta_{i,4}$, the amount of angular material required to satisfy developability. If $\theta_{i,1} = \pi/2$, we have $\cos\theta_{i,2} = \sin\beta_i\cos\alpha_i$, which yields a unique solution if $\beta_i \neq 0, \pi$ and $\beta_i < k_i < 2\pi - \beta_i$ (see *SI Appendix*, section S1 for details). We thus see that the solutions $\theta_{i,1}, \theta_{i,2}$ to Eqs. **1** and **2** exist and are unique for any given $\theta_{i,3}$, $\theta_{i,4}$ and β_i (angles intrinsic to the existing origami) and α_i (the flap angle), modulo a finite number of singular configurations. The new transverse edge direction $\mathbf{r}_i$ can then be obtained by using $\theta_{i,1}$ and $\theta_{i,2}$ (Fig. 1*E*). The key geometric intuition and an alternative proof of existence and uniqueness of single-vertex solutions is to observe that k_i defines an ellipse γ_i of spherical arcs $\theta_{i,1}, \theta_{i,2}$ that satisfies Eq. **1** with foci given by $-\mathbf{e}_i$ and $\mathbf{e}_{i+1}$. For any flap angle α_i, the sum $\theta_{i,1} + \theta_{i,2} = \beta_i$ when $\theta_{i,1} = 0$ and $\theta_{i,1} + \theta_{i,2} = 2\pi - \beta_i$ when $\theta_{i,1} = \pi$ and the sum $\theta_{i,1} + \theta_{i,2}$ is positive monotonic on the interval $\theta_{i,1} \in [0, \pi]$, generically. Moreover, the spherical triangle inequality bounds $\beta_i < \theta_{i,3} + \theta_{i,4} < 2\pi - \beta_i$ generically, so no matter what flap angle is chosen or inherited from a neighboring vertex, a unique solution to Eqs. **1** and **2** must exist, and the flap angle α_i parameterizes the ellipse γ_i. See *SI Appendix*, section S1 and Movie S1 for further details and discussion.

2. Construction of adjacent vertices: We now show that the new edge directions $\mathbf{r}_{i+1}$, $\mathbf{r}_{i-1}$ at $\mathbf{x}_{i+1}$, $\mathbf{x}_{i-1}$ are also uniquely determined by the single flap angle α_i. Without loss of generality, consider obtaining $\mathbf{r}_{i+1}$ given $\mathbf{r}_i$ (Fig. 1*F*). Denote α_i' as the left-hand-oriented angle about $\mathbf{e}_{i+1}$ from the β_i plane to the plane of the new quad containing $\theta_{i,2}$. Referring again to the spherical triangle formed by $\theta_{i,1}$, $\theta_{i,2}$ and β_i, the spherical laws of sines and cosines give

$$\sin\alpha_i' = \frac{\sin\theta_{i,1}(\alpha_i)}{\sin\theta_{i,2}(\alpha_i)}\sin\alpha_i, \qquad \textbf{[5]}$$

$$\cos\alpha_i' = \frac{\cos\theta_{i,1}(\alpha_i) - \cos\theta_{i,2}(\alpha_i)\cos\beta_i}{\sin\theta_{i,2}(\alpha_i)\sin\beta_i}, \qquad \textbf{[6]}$$

yielding a unique solution $\alpha_i' \in [0, 2\pi)$. As $\theta_{i,1}$ and $\theta_{i,2}$ are functions of α_i, α_i' is also a function of α_i. Observe that α_i' and α_{i+1} are measured about a common axis and are thus related by a shift of the left-hand-oriented angle τ_i from the β_i face to the β_{i+1} face. This gives the flap-angle transfer function $g_i : [0, 2\pi) \to [0, 2\pi)$:

$$\alpha_{i+1} = g_i(\alpha_i) = \mathrm{mod}(\alpha_i'(\alpha_i) - \tau_i, 2\pi), \qquad \textbf{[7]}$$

as measured left-hand-oriented about $\mathbf{e}_{i+1}$ starting at the β_i plane. It is easy to see that g is bijective; hence, $\mathbf{r}_{i+1}$ is uniquely determined by α_i, and both γ_i and γ_{i+1} are parameterized by α_i (Fig. 1*G*). A similar argument applies for $\mathbf{r}_{i-1}$. For geometric intuition, observe that there are bijections between points on γ_i and the half-planes about $\mathbf{e}_i$ and $\mathbf{e}_{i+1}$.

3. Growth of the entire front: Finally, to establish bijection between the flap angles α_i and α_j at arbitrary i, j, where $i < j$, we consider the following composition $f_{i,j}$ of the transfer functions g:

$$\alpha_j = f_{i,j}(\alpha_i) = g_j(g_{j-1}(g_{j-2}(\cdots g_i(\alpha_i)))). \qquad \textbf{[8]}$$

Since each transfer function is bijective, their composition is also bijective. Therefore, all new interior edge directions along the entire growth front are parameterized by a single flap angle α_i. ■

Corollary. *Given a generic curve* $\mathcal{C}$ *discretized by* $m+1$ *vertices* $\mathbf{x}_i \in \mathbb{R}^3$, $i = 0, \ldots, m$ *and* m *edges* $\mathbf{e}_i = \mathbf{x}_i - \mathbf{x}_{i-1}$, $i = 1, \ldots, m$, *with angles* $\beta_i = \angle\{-\mathbf{e}_i, \mathbf{e}_{i+1}\} \in (0, \pi)$, $i = 1, \ldots, m-1$, *the space of planar patterns that fold to* $\mathcal{C}$ *is* m*-dimensional.*

Proof: Consider assigning $k_i \in (\beta_i, 2\pi - \beta_i)$, $i = 1, \ldots, m-1$ to the interior vertices of $\mathcal{C}$. In the above origami proof, $\mathcal{C}$ is a growth front, and k_i is given by the existing origami surface. For a discrete curve, k_i can be chosen freely to determine a one-dimensional set of fold directions $\mathbf{r}_i \in \mathbb{R}^3$, $i = 1, \ldots, m-1$ that give a development of $\mathcal{C}$ to the plane. ■

This proof suggests immediately an efficient geometric algorithm for designing generic quad origami surfaces. For an existing regular quad origami (seed) with a growth front designated by a strip of m boundary quads (Fig. 2*A*), we note that a new strip of m quads has $3(m+1)$ DOFs in $\mathbb{R}^3$ subject to m planarity and $m-1$ design angle constraints. If we add a new strip to a boundary with m quads, we have a total of $m+4$ DOFs to determine the geometry of the new strip: one flap angle to determine the interior design angles and edge directions, two boundary-design angles at the endpoints of the strip, and $m+1$ edge lengths. So while our main theorem establishes the design space of generic quad origami, the following geometric algorithm allows us to explore this landscape additively, satisfying developability constraints by construction along the way. A new compatible strip of m quads is designed by the following steps.

1. Start from any $i \in \{1, 2, \ldots, m-1\}$ and choose the flap angle α_i associated with the growth-front edge $\mathbf{e}_i$ (one DOF) (Fig. 2*B*).
2. Propagate the α_i choice along the growth front from $\mathbf{x}_i$ to $\mathbf{x}_1$ and $\mathbf{x}_{m-1}$ by iteratively solving for $\theta_{i,1}, \theta_{i,2}$, rotating $\mathbf{r}_i$, calculating $\alpha_{i-1}, \alpha_{i+1}$, and moving on to the next vertex (Fig. 2*C*).
3. Choose boundary-design angles $\theta_{0,2}, \theta_{m,1} \in (0, \pi)$ and rotate $\mathbf{r}_0$ and $\mathbf{r}_m$ into position (two DOFs) (Fig. 2*D*).
4. Calculate the new edge-length bounds and choose l_j for all j ($m+1$ DOFs). Bounds are given by the observation that the new outward-facing edges in each new quad cannot intersect

APPLIED PHYSICAL SCIENCES

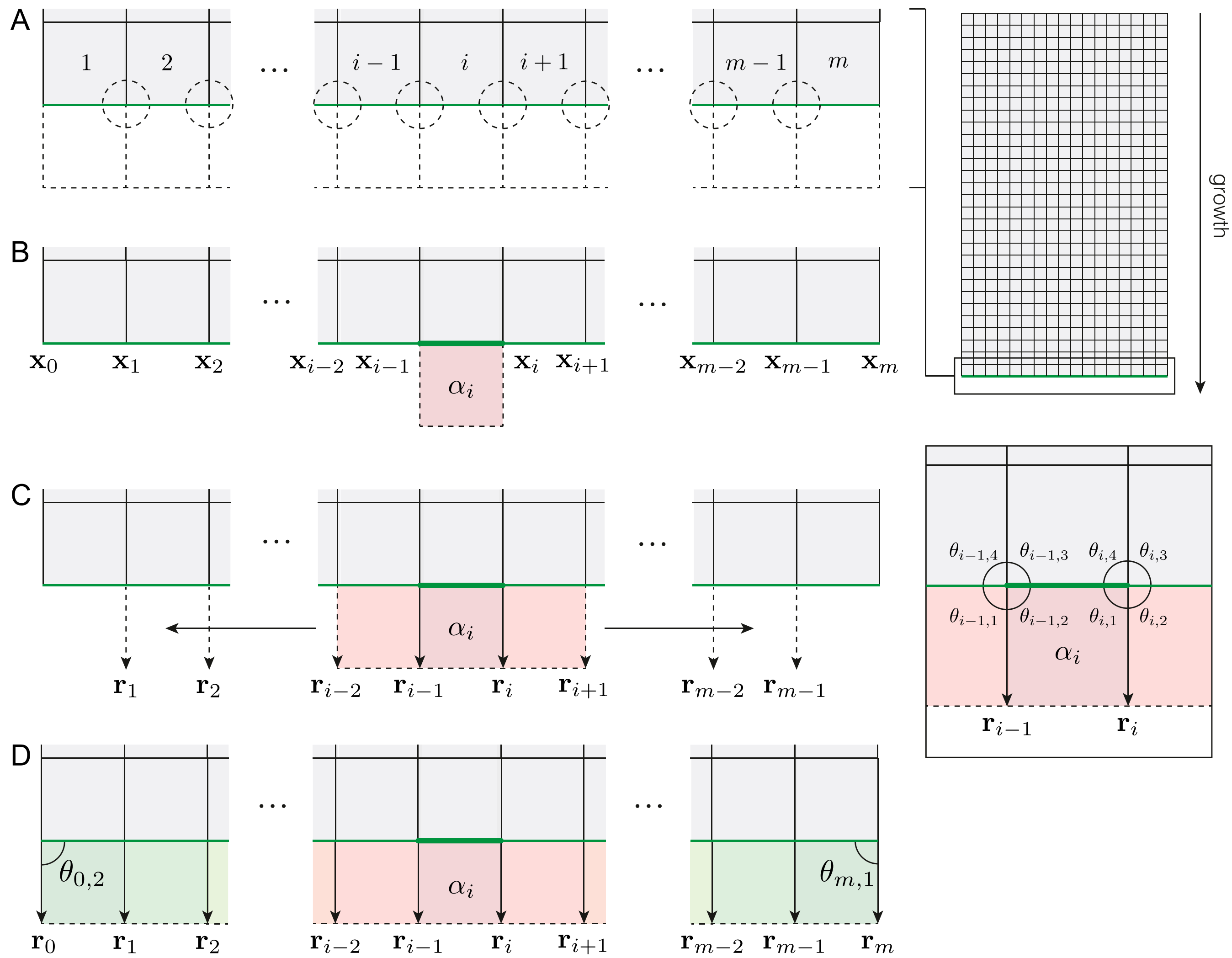

Fig. 2. Additive algorithm. (*A*) To grow an existing folded quad origami model at a boundary having m quads, $m+1$ new vertices must be placed in space, subject to m planarity constraints (dashed squares) and $m-1$ angle sum constraints (dashed circles), for a total of $3(m+1)-(2m-1)=m+4$ DOFs, generically. (*B*) The additive strip construction begins by choosing the plane associated with any one of the quad faces in the new strip (one DOF). (*C*) Consecutive single-vertex systems propagate this flap-angle choice down the remainder of the strip, determining uniquely the orientations in space of all quad faces in the new strip. (*D*) Edge directions at the endpoints of the strip can be chosen freely in their respective planes (two DOFs), and all transverse edges in the new strip can be assigned lengths ($m+1$ DOFs) for a total $m+4$ DOFs.

each other, which occurs when the two interior angles of a new quad sum to less than π (*SI Appendix*, section S3).

5. Calculate the new vertex positions given $\mathbf{r}_j$ and l_j for all j.
6. Repeat the above steps at any boundary front to grow more new strips.

The algorithm also applies to discrete curves not associated with an existing folded surface via the corollary. In this case, we can design the shape of the development of the curve by choosing k values in step 2, rather than calculating them from an existing surface.

Having established generic connections from single vertices to quad strips to origami surfaces, we now analyze the flap-angle parameterization at each scale of this hierarchy in more detail. The design space of the growth front of a pair of folded faces, a proto-single-vertex origami, is described fully by the pair of scalars β, the angle in space formed by the growth front, and k, the shape parameter of γ—i.e., the amount of angular material required to satisfy developability (Fig. 3*A*). A generic single-vertex origami can be constructed in the interior of the triangular region $0 \leq \beta \leq \pi$ and $\beta \leq k \leq 2\pi - \beta$, with singular configurations at the boundaries given by equality (Fig. 3*B*). Sweeping α from zero to 2π parameterizes the ellipse such that $\theta_1(\alpha = 0) = (k+\beta)/2$ and $\theta_1(\alpha = \pi) = (k-\beta)/2$, and new edge directions $\mathbf{r}(\alpha)$ tend to cluster in space around growth-front directions, where $d\theta_1/d\alpha$ has smaller magnitude. Special single-vertex origami (40) are recovered by identifying their flap angles (Fig. 3*A*; see *SI Appendix* for formulae). Three of these vertex types are given by rearranging Eq. **3** and plugging in a desired value for the new design angle: the continuation solution α_{con}, where the new pair of quads can be attached without creating a new fold; the flat-foldable solution α_{ff}, where the vertex can be fully folded such that all faces are coplanar; and α_{eq}, which creates equal new design angles. These each admit two solutions related by reflection over the plane of the growth front, recovering a duality noted in ref. 5. Two more special vertices are identified by α_{ll} and α_{lr}, which produce locked configurations with the left pair of faces (θ_1, θ_4) and the right pair (θ_2, θ_3) folded to coplanarity, respectively. A vertex is trivially locked with coplanar (θ_1, θ_2) faces when $\alpha = 0, \pi$. The continuation flap angle that does not create a new fold along the growth front and

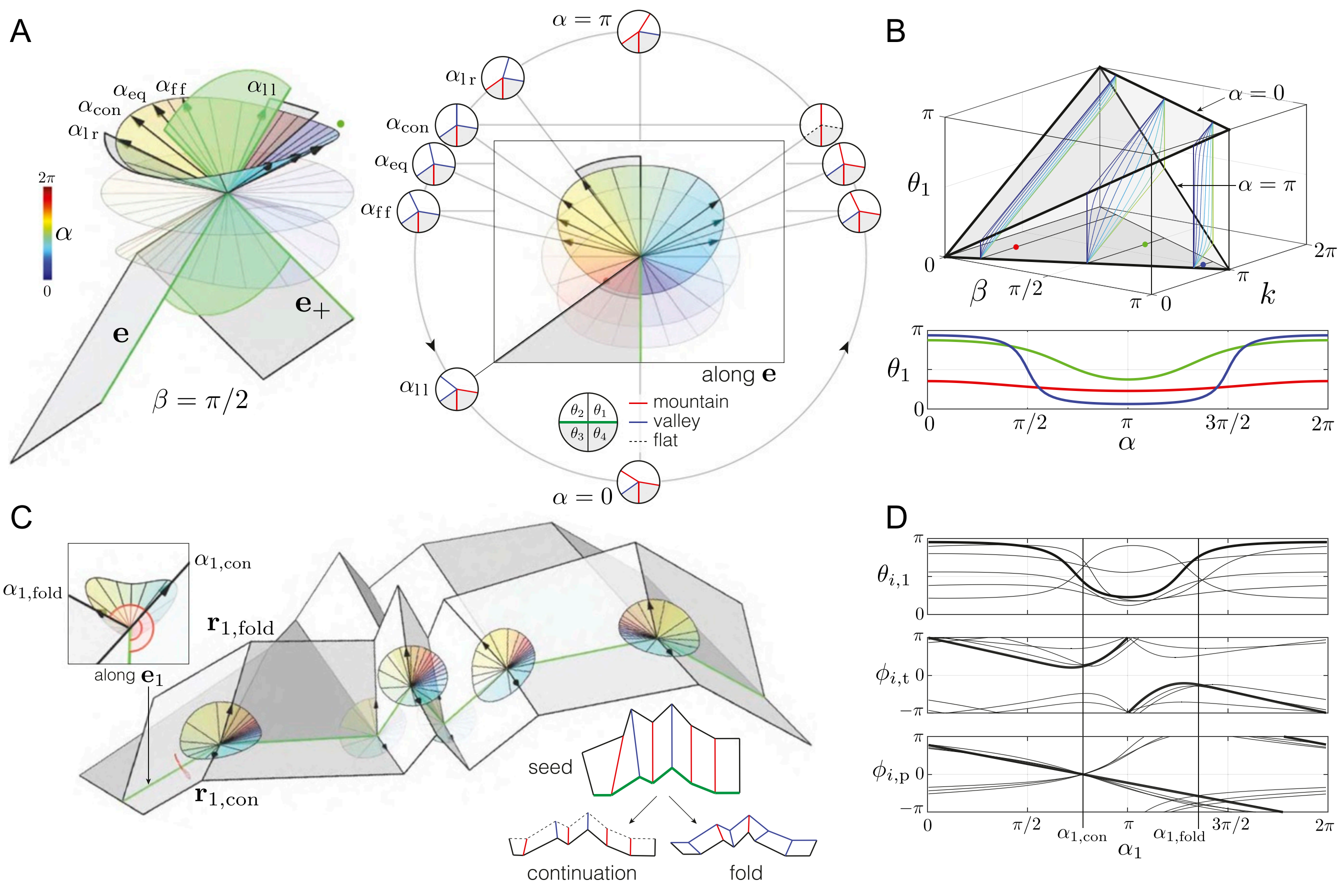

Fig. 3. Vertex and strip design. (*A*) A pair of folded quads and their single-vertex growth front with $\beta = \pi/2$ and the spherical ellipse given by $k = 5\pi/4$ are shown, along with two other faint ellipses given by $k = \pi, 3\pi/4$ that would be given by different existing design angles than those shown. Special vertex growth directions and self-intersection intervals are recovered by identifying their flap angles, three of which (α_{con}, α_{eq}, α_{ff}) have two solutions given by reflection over the β plane. (*B*, *Upper*) Valid region for β and k at a single vertex. Typical generic growth-front vertices (red, green, and blue points) fall in the interior of this region. The first design angle θ_1 is bounded above by $(k+\beta)/2$ at $\alpha = 0$ and below by $(k-\beta)/2$ at $\alpha = \pi$, and surfaces of constant α are shown in the interstice. Sweeping $\alpha \in [0, 2\pi)$ produces possible values for θ_1 (*B*, *Lower*) symmetric about $\alpha = \pi$ for the three colored points identified above. (*C*) A folded quad strip with two compatible growth directions (continuation, where no new fold is created, and a folded configuration) selected from the one-dimensional space of compatible strip designs parameterized by the orientation in space of the first new face. (*D*) Half of the new interior design angles $\theta_{i,1}$ in the new strip (*Top*), fold angles transverse to the growth front $\phi_{i,t}$ (*Middle*), and parallel to the growth front $\phi_{i,p}$ (*Bottom*) are shown as functions of flap angle α_1. Characteristic single-vertex curves associated with $\mathbf{x}_1$ are bolded, while curves associated with other vertices (light black) differ from characteristic single-vertex curve shapes by nonlocality.

the locked-left flap angle are related by $\alpha_{con} = \mathrm{mod}(\alpha_{ll} + \pi, 2\pi)$. We also note that self-intersection will occur for flap angles in the intervals between the β plane and the nearest nontrivial locked flap angle. Notably absent from our construction are fold angles, which can be recovered at growth-front edge $\mathbf{e}_i$ by $\phi_{i,p} = \alpha_{i,ll} - \alpha_i - \pi$.

Moving up in scale, we explore the relationship between flap angle and strip design. The special single-vertex solutions cannot necessarily be enforced at all locations along a generic surface growth front, as the space of growth directions is one-dimensional. To design a set of flat-foldable growth-front folds, for example, requires additional symmetries. The exception to this is $\alpha_{i,con}$, the single flap-angle value that gives the trivial growth direction for the entire front. In Fig. 3*C*, we illustrate a generic folded quad strip and two of its compatible strips, the trivial continuation solution and a nontrivial folded solution. New design angles $\theta_{i,1}$, fold angles transverse to the growth front $\phi_{i,t}$ and parallel to the growth front $\phi_{i,p}$ in the new strip, are shown as functions of flap angle α_1 in Fig. 3*D*. Fold angles parallel to the growth front $\phi_{i,p}$ are simultaneously zero at $\alpha_{1,con}$ and nonzero otherwise, while fold angles transverse to the growth front $\phi_{i,t}$ are generically never zero. See *SI Appendix*, section S2 and Movies S2 and S3 for more details.

To show the capability of our additive approach, we now deploy it in inverse design frameworks to construct ordered and disordered quad origami typologies with straight and curved folds. In contrast with previous work (32), our additive approach does not require the solution of a large multidimensional optimization problem for the entire structure. Instead, it only requires choosing from the available DOFs for each strip, which map the full space of compatible designs, and hence is more computationally feasible and geometrically complete. These choices are application-specific and can be random, interactive, or based on some optimization criteria.

As our first example, we consider the approximation of a doubly curved target surface using a generalized Miura-ori tessellation. Given a smooth target surface that we want to approximate, we consider two bounding surfaces displaced in the normal direction from the target surface (an upper and a lower bound) and construct a simple, singly corrugated strip in their interstice with one side of the strip lying on the upper surface and one side on the lower surface (see *SI Appendix*, section S4A for more details). Then, applying our additive algorithm, we add strips to either side of the seed (and continuing on the growing patch) that approximately reflect the origami surface back and forth between the upper and lower target bounds, inducing an additional corrugation in a transverse direction to that of the corrugation in the seed. Fig. 4*A* shows a high-resolution generalized Miura-ori sandwich structure of constant thickness obtained by our approach that approximates a mixed-curvature landscape, which would be very difficult to obtain using current techniques. As our second example, using a different DOF selection setup with no reference target surface, we grow a conical seed with a series of straight ridges with fourfold symmetry via facets that are created by reflections back and forth between a pair of rotating planes, shown in Fig. 4*B*. As our third example, we turn to designing surfaces that have curve folds, folds that approximate a smooth spatial curve with nonzero curvature and torsion (5). Fig. 4*C* shows a twisted version of David Huffman's *Concentric Circular Tower* (41) obtained by our method, which uses a similar DOF selection setup as Fig. 4*B*, but begins with a high-resolution cone segment as the inner-ring seed and follows with progressively thicker tilted cone rings added transversely (see *SI Appendix*, section S4B for more details on both of these models). Fig. 4*D* shows another curved-fold model that uses the corollary to create a seed from a corrugated discrete planar parabola and proceeds to add new strips with constant flap angles and edge lengths, growing in a direction along the folds (see *SI Appendix*, section S4C for more details). As our last surface example, we use our approach to create a disordered, crumpled surface that is isometric to the plane, again a structure that would be very difficult to obtain using current techniques. For each step of strip construction in the additive algorithm, the flap angle and edge lengths can be chosen randomly, thereby leading to a crumpled sheet that does not follow a prescribed MV pattern (Fig. 4*E*). To model the physically realizable crumpled geometry, we have chosen flap angles according to the self-intersection bounds given by special vertex solutions along the entire front, so that the growth of the sheet is a locally self-avoiding walk (see *SI Appendix*, section S4D for more details).

Finally, to emphasize the flexibility of the corollary, we construct a quad strip that forms a folding connection between a canonically rough structure, a random walk in three dimensions (3D), and a canonically smooth structure, a circle in two dimensions (2D). Fig. 4*F* shows a single folded strip generated by sampling a discrete Brownian path in 3D to form one boundary of a folded strip, choosing k values such that its development falls on a circle and forms a single closed loop for any choice of flap-angle value and choosing edge lengths such that the other boundary of the strip develops to another, smaller concentric circle (*SI Appendix*, section S4E). Indeed, the corollary allows for the freeform design of both folded ribbons and their pattern counterparts independently. See Movies S4–S9 for 3D animations of the models in Figs. 4 and *SI Appendix*, Figs. S11, S12, S14, S16, and S17 for a gallery of other surface-fitting, curved-fold, disordered, and Brownian ribbon results obtained by our additive approach.

Since the developability condition in Eq. **1** is always satisfied in our marching algorithm, all physical models created by it that do not self-intersect can transform from a 2D flat state to the isometric 3D folded state, typically through an energy

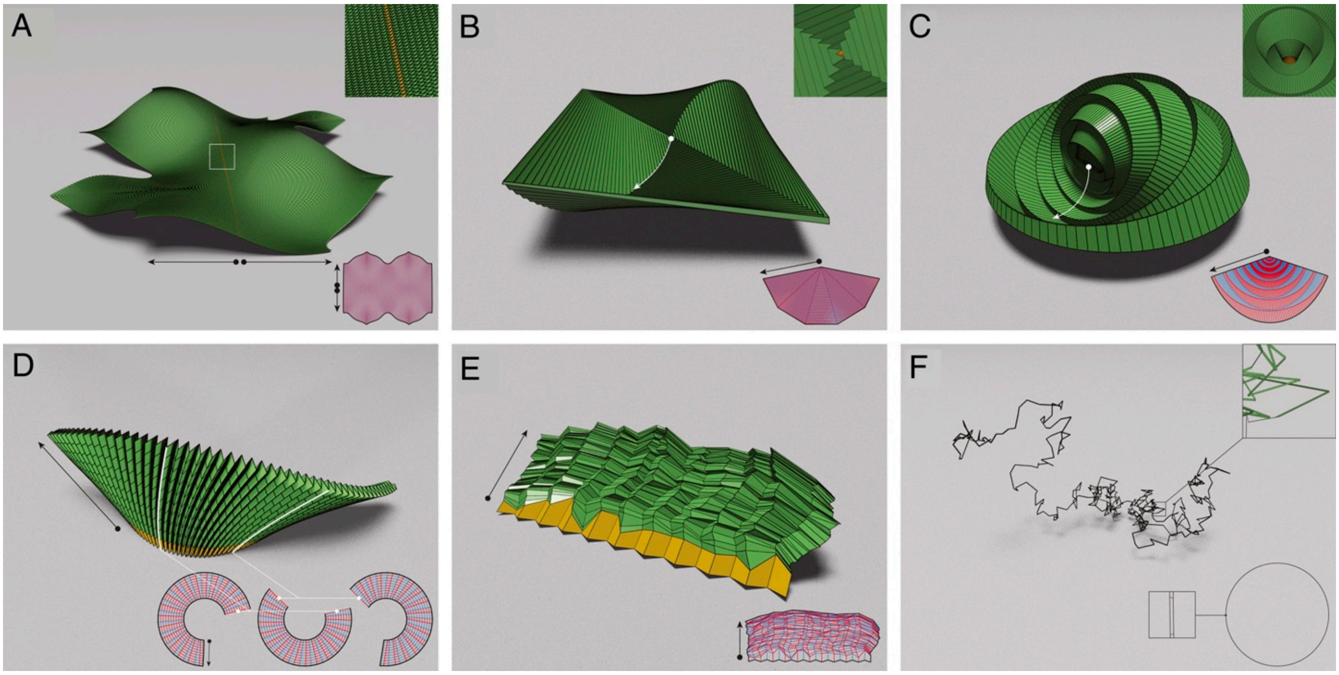

Fig. 4. Additive design of straight, curved, ordered, and disordered origami. (*A*) A generalized Miura-ori tessellation fit to a target surface with mixed Gaussian curvature generated. Lower and upper bounding surfaces are displaced normally from the target surface, and a seed strip of quads is initialized in between the two with one growth front on each surface. New strips are attached on either side of the seed by reflecting the growth front back and forth between bounding surfaces in their interstice. (*B*) A low-resolution conical seed with fourfold symmetry grows by reflecting between the interstices of two rotating upper and lower boundary planes. New strips form closed loops with overlapping endpoint faces. (*C*) A high-resolution conical seed grows by attaching progressively tilted cone rings to reproduce a curved-fold model. New strips form closed loops with overlapping endpoint faces. (*D*) A curved-fold model grows from a seed created by using the corollary to attach a strip of quads to a corrugated parabola. (*E*) A self-avoiding walk away from a Miura-ori seed strip with noise added to the boundary growth front produces a crumpled sheet. New strips are added by sampling flap angles within bounds that prevent local self-intersection. (*F*) A Brownian ribbon whose development approximates a circular annulus is created by using the corollary. The seeds are highlighted in yellow, and the arrows indicate the growth direction. The fold pattern for each model is shown at the bottom right of each image. The *Upper Right Insets* in *A*–*C* and *F*, along with the small square next to the pattern in *F*, are zoomed-in views to highlight details. See *SI Appendix*, Figs. S8 and S9 for higher-resolution versions of the fold patterns.

landscape that includes geometric frustration (see *SI Appendix*, section S5 and Fig. S18 and Movie S10 for folding simulations). Because the landscape depends on the geometry of the folding pattern for which folding motions are not unique, this opens future routes to also program metastability. We also note that by replacing the right side in Eq. **1** by $K \neq 2\pi$ and suitably modifying the subsequent trigonometric formulas, our additive approach generalizes to the design of non-Euclidean origami (42, 43), with solutions uniquely existing in the same way when $K - \theta_{i,3} - \theta_{i,4} \in (\beta_i, 2\pi - \beta_i)$.

Overall, our study provides a unified framework for the inverse design of generic developable quad origami patterns and discrete developable surfaces via growth. A simple theorem forms the basis for a marching algorithm that replaces the solution of a difficult global optimization problem with a scalable, easy-to-implement scheme for the evolution of a constrained folded front. This interplay between bulk rigidity and boundary flexibility that allows us to rapidly prototype computational designs of ordered, disordered, straight-, and curved-folded geometries holds substantial promise for advances in discrete geometry, engineering applications, and artistic creations alike.

Data Availability. Some study data are available in GitHub at https://github.com/garyptchoi/additive-origami.

ACKNOWLEDGMENTS. This work was supported in part by the Harvard Quantitative Biology Initiative and the NSF-Simons Center for Mathematical and Statistical Analysis of Biology at Harvard, Award 1764269 (to G.P.T.C. and L.M.); and NSF Grants DMR-2011754 (to L.M.), DMR-1922321 (to L.M.), and EFRI-1830901 (to L.M.).

1. H. Kobayashi, B. Kresling, J. F. V. Vincent, The geometry of unfolding tree leaves. *Proc. R. Soc. B* **265**, 147–154 (1998).
2. N. Bowden, S. Brittain, A. G. Evans, J. W. Hutchinson, G. M. Whitesides, Spontaneous formation of ordered structures in thin films of metals supported on an elastomeric polymer. *Nature* **393**, 146–149 (1998).
3. L. Mahadevan, S. Rica, Self-organized origami. *Science* **307**, 1740 (2005).
4. A. E. Shyer *et al.*, Villification: How the gut gets its villi. *Science* **342**, 212–218 (2013).
5. D. A. Huffman, Curvature and creases: A primer on paper. *IEEE Trans. Comput.* **10**, 1010–1019 (1976).
6. K. Liu, T. Tachi, G. H. Paulino, Invariant and smooth limit of discrete geometry folded from bistable origami leading to multistable metasurfaces. *Nat. Commun.* **10**, 1–10 (2019).
7. A. Lebée, L. Monasse, H. Nassar, "Fitting surfaces with the Miura tessellation" in *The 7th International Meeting on Origami in Science, Mathematics and Education (7OSME)*, R. J. Lang, M. Bolitho, Z. You, Eds. (Tarquin Group, St Albans, United Kingdom, 2018), p. 811.
8. E. D. Demaine, J. O'Rourke, *Geometric Folding Algorithms: Linkages, Origami, Polyhedra* (Cambridge University Press, Cambridge, UK, 2007).
9. R. J. Lang, *Origami Design Secrets: Mathematical Methods for an Ancient Art* (CRC Press, Boca Raton, FL, 2011).
10. M. A. Dias, L. H. Dudte, L. Mahadevan, C. D. Santangelo, Geometric mechanics of curved crease origami. *Phys. Rev. Lett.* **109**, 114301 (2012).
11. Z. Y. Wei, Z. V. Guo, L. Dudte, H. Y. Liang, L. Mahadevan, Geometric mechanics of periodic pleated origami. *Phys. Rev. Lett.* **110**, 215501 (2013).
12. B. Liu *et al.*, Topological kinematics of origami metamaterials. *Nat. Phys.* **14**, 811–815 (2018).
13. C. D. Santangelo, Extreme mechanics: Self-folding origami. *Annu. Rev. Condens. Matter Phys.* **8**, 165–183 (2017).
14. E. T. Filipov, T. Tachi, G. H. Paulino, Origami tubes assembled into stiff, yet reconfigurable structures and metamaterials. *Proc. Natl. Acad. Sci. U.S.A.* **112**, 12321–12326 (2015).
15. Y. Chen, R. Peng, Z. You, Origami of thick panels. *Science* **349**, 396–400 (2015).
16. E. D. Demaine, T. Tachi, "Origamizer: A practical algorithm for folding any polyhedron" in *33rd International Symposium on Computational Geometry (SoCG 2017)*, B. Aronov, M. J. Katz, Eds. (Schloss Dagstuh, Wadern, Germany, 2017), vol. 34, pp. 1–5.
17. S. J. P. Callens, A. A. Zadpoor, From flat sheets to curved geometries: Origami and kirigami approaches. *Mater. Today* **21**, 241–264 (2018).
18. Z. He, S. D. Guest, "Approximating a target surface with 1-DOF rigid origami" in *The 7th International Meeting on Origami in Science, Mathematics, and Education (7OSME)*, R. J. Lang, M. Bolitho, Z. You, Eds. (Tarquin Group, St Albans, United Kingdom, 2018), vol. 2, pp. 505–520.
19. M. B. Pinson *et al.*, Self-folding origami at any energy scale. *Nat. Commun.* **8**, 15477 (2017).
20. S. Chen, L. Mahadevan, Rigidity percolation and geometric information in floppy origami. *Proc. Natl. Acad. Sci. U.S.A.* **116**, 8119–8124 (2019).
21. K. Miura, *Method of Packaging and Deployment of Large Membranes in Space* (The Institute of Space and Astronautical Science Report, Institute of Space and Astronautical Science, Yoshinodai, Sagamihara, Kanagawa, Japan, 1985), vol. 618.
22. J. Mitani, A design method for 3D origami based on rotational sweep. *Comput. Aided Des. Appl.* **6**, 69–79 (2009).
23. J. M. Gattas, W. Wu, Z. You, Miura-base rigid origami: Parameterizations of first-level derivative and piecewise geometries. *J. Mech. Des.* **135**, 111011 (2013).
24. J. M. Gattas, Z. You, Miura-base rigid origami: Parametrizations of curved-crease geometries. *J. Mech. Des.* **136**, 121404 (2014).
25. X. Zhou, H. Wang, Z. You, Design of three-dimensional origami structures based on a vertex approach. *Proc. R. Soc. A* **471**, 20150407 (2015).
26. P. Sareh, S. D. Guest, Design of isomorphic symmetric descendants of the Miura-ori. *Smart Mater. Struct.* **24**, 085001 (2015).
27. F. Wang, H. Gong, X. Chen, C. Q. Chen, Folding to curved surfaces: A generalized design method and mechanics of origami-based cylindrical structures. *Sci. Rep.* **6**, 33312 (2016).
28. K. Song, X. Zhou, S. Zang, H. Wang, Y. Zhong, Design of rigid-foldable doubly curved origami tessellations based on trapezoidal crease patterns. *Proc. R. Soc. A* **473**, 20170016 (2017).
29. Y. Hu, H. Liang, H. Duan, Design of cylindrical and axisymmetric origami structures based on generalized Miura-ori cell. *J. Mech. Robot.* **11**, 051004 (2019).
30. F. Feng, P. Plucinsky, R. D. James, Helical Miura origami. *Phys. Rev. E* **101**, 033002 (2020).
31. T. Tachi, Generalization of rigid-foldable quadrilateral-mesh origami. *J. Int. Assoc. Shell Spat. Struct.* **50**, 173–179 (2009).
32. L. H. Dudte, E. Vouga, T. Tachi, L. Mahadevan, Programming curvature using origami tessellations. *Nat. Mater.* **15**, 583–588 (2016).
33. M. Kilian *et al.*, Curved folding. *ACM Trans. Graph.* **27**, 75 (2008).
34. C. Jiang, K. Mundilova, F. Rist, J. Wallner, H. Pottmann, Curve-pleated structures. *ACM Trans. Graph.* **38**, 169 (2019).
35. R. J. Lang, L. Howell, Rigidly foldable quadrilateral meshes from angle arrays. *J. Mech. Robot.* **10**, 021004 (2018).
36. P. Dieleman, N. Vasmel, S. Waitukaitis, M. van Hecke, Jigsaw puzzle design of pluripotent origami. *Nat. Phys.* **16**, 63–68 (2020).
37. F. Feng, X. Dang, R. D. James, P. Plucinsky, The designs and deformations of rigidly and flat-foldable quadrilateral mesh origami. *J. Mech. Phys. Solids* **142**, 104018 (2020).
38. T. Fuse, *Unit Origami: Multidimensional Transformations* (Japan Publications, Tokyo, Japan, 1990).
39. L. H. Dudte, "Inverse design of shape using folds and cuts in flat sheets," PhD thesis, Harvard University, Cambridge, MA (2017).
40. S. Waitukaitis, M. Van Hecke, Origami building blocks: Generic and special four-vertices. *Phys. Rev. E* **93**, 023003 (2016).
41. The Institute for Figuring, Curved crease origami. http://www.theiff.org/oexhibits/paper04.html. Accessed 18 October 2019.
42. M. Berry, M. E. Lee-Trimble, C. D. Santangelo, Topological transitions in the configuration space of non-Euclidean origami. *Phys. Rev. E* **101**, 043003 (2020).
43. S. Waitukaitis, P. Dieleman, M. Van Hecke, Non-Euclidean origami. *Phys. Rev. E* **102**, 031001 (2020).